Structural and elastic properties of $LaAlO_3$ from first-principles calculations

Xin Luo and Biao Wang

Citation: Journal of Applied Physics **104**, 073518 (2008); doi: 10.1063/1.2990068
View online: http://dx.doi.org/10.1063/1.2990068
View Table of Contents: http://aip.scitation.org/toc/jap/104/7
Published by the American Institute of Physics

Structural and elastic properties of $LaAlO_3$ from first-principles calculations

Xin Luo and Biao Wang[a)]
State Key Laboratory of Optoelectronic Materials and Technologies/Institute of Optoelectronic and Functional Composite Materials, School of Physics and Engineering, Sun Yat-sen University, Guangzhou, People's Republic of China

(Received 26 May 2008; accepted 11 August 2008; published online 6 October 2008)

Using the first-principles linearized augmented plane wave calculations within density functional theory, the stable structure, the phase transition, and elastic properties of the $LaAlO_3$ are investigated. At low temperature, our calculation indicates that the rhombohedral *R*-3*C* phase is the most energetically stable structure among the three proposed structures: *R*-3*C* (No. 167), *R*-3*M* (No. 166), and *R*3*C* (No. 161). It is found that the $LaAlO_3$ transforms from rhombohedral *R*-3*C* phase to cubic *PM*-3*M* phase with a volume change of 1% when the applied hydrostatic pressure is 15.4 GPa, which is consistent with the experimental value. The elastic constants, shear modulus, bulk modulus, and Poisson's ratio of $LaAlO_3$ are calculated and compared with corresponding experimental data. Our result shows that the rotation of the AlO_6 octahedra in $LaAlO_3$ has a large influence on the anisotropic elastic constants. From the calculated Debye temperature and elastic constants, the *R*-3*C* phase of $LaAlO_3$ is predicted to be more thermostable and to exhibit higher fracture toughness than the high-pressured *PM*-3*M* phase. © *2008 American Institute of Physics*. [DOI: 10.1063/1.2990068]

I. INTRODUCTION

Lanthanum aluminate ($LaAlO_3$), with its elegant perovskite-type structure, is a popular target of fundamental investigation, since it exhibits a wide variety of physical and mechanical properties when the applied conditions are changed. For a long time, the $LaAlO_3$ has been extensively used as the substrate material for the growth of functional thin films such as the $SiTiO_3$,[1] $Nd_{0.7}Sr_{0.3}MnO_3$ (Ref. 2) and so on. Due to its moderate dielectric properties, $LaAlO_3$ is also widely used in the superconducting microwave devices.[3,4] At present, $LaAlO_3$ has been the subject of study due to its new identity as a promising candidate for the high *k* gate oxide, which is intended to replace silicon dioxide (SiO_2) in the metal-oxide-semiconductor field-effect-transistor (MOSFET) application.[5] With the ongoing miniaturization in the semiconductor industry, the thickness of conventional SiO_2 layer is approaching its physical limit, due to its large tunneling leakage current.[6] Whereas, the single crystalline $LaAlO_3$ has a proper dielectric constant ($\varepsilon \sim 25$),[7] large optical band gap (6.2 eV),[8] and stable thermal property during the MOSFET annealing process.[9] Moreover, the conduction and valence band offsets of the $LaAlO_3$ films on Si are measured to be 2.52 and 2.86 eV, respectively.[10] It was also found that the Si thin film could grow epitaxially on the $LaAlO_3$ substrate with an atomically well defined interface.[11]

Since the early work of Wood,[12] $LaAlO_3$ has been known to undergo a phase transition from the low temperature rhombohedral phase to a cubic phase at high temperature. However, conflicting references are found for the $LaAlO_3$ low temperature phase. In the pioneering work of Geller and Bala,[13] a crystallographic analysis of the rhombohedral *R*-3*M* to cubic *PM*-3*M* phase transition was made. With refined equipment, the *R*-3*M* structure at room temperature was reproduced in later literature[14] and frequently quoted by other works. However, detailed works on the soft-mode mechanism of the phases transition revealed that the *R*-3*C* phase is more likely to be the $LaAlO_3$ low temperature structure,[15–17] and their works were confirmed by the latter neutron powder diffraction study.[18] Recently, the resonant Raman spectroscopy study expressed doubts about the hitherto assumed *R*-3*C* structure because of extra observed Raman bands,[19] and a local breakdown symmetry with space group *R*3*C*/*R*-3 for $LaAlO_3$ was proposed as its low temperature structure. Therefore, it seems that the crystal structure of $LaAlO_3$ at low temperature is still a disputable issue and requires further analysis.

In order to better control the thermodynamic performance of the $LaAlO_3$ thin film in the nanoelectronic devices, it is important to understand the low temperature stable structure of $LaAlO_3$ and its elastic properties in different directions. At present, we could not find any theoretical calculation of such elastic constants of $LaAlO_3$. In this paper, we will consider the possible stable structures of $LaAlO_3$ via the energy minimum analysis from the first-principles calculation. Then the phase transition behavior of $LaAlO_3$ under external hydrostatic pressure is investigated. After that we focus on the elastic properties of different phases of $LaAlO_3$. A detailed analysis of the elastic constants is given by both generalized gradient approximation (GGA) and local density approximation (LDA) calculations, following the approach described by Ravindran *et al.*[20] Finally, the wave velocity, Debye temperature, and other elastic properties are also deduced from the basic elastic constants and compared to corresponding experimental data.

[a)]Author to whom correspondence should be addressed. Electronic mail: wangbiao@mail.sysu.edu.cn.

TABLE I. The calculated formation energies and structural parameters of $LaAlO_3$ after structural relaxation.

Configuration	ΔE (eV/unit cell)	a(Å)	c(Å)	V(Å^3)	$\bar{d}_{La-O}$(Å)	$\bar{d}_{Al-O}$(Å)	$\bar{d}_{O-O}$(Å)
R-3*C*	−2.342	5.370	13.139	328.071	2.675	1.899	2.686
Expt.		5.365[a]	13.110[a]	326.732[a]	2.682[b]	1.901[b]	
R-3*M*	−2.244	5.366	13.143	327.685	2.683	1.897	2.683
Expt.		5.365[c]	13.112[c]	326.845[c]			
*R*3*C*	−2.061	5.372	13.138	328.305	2.624	1.900	2.684
PM-3*M*	−2.284	3.753		52.870	2.650	1.877	2.650
Expt.		3.715[d]		51.286[d]	2.652[b]	1.878[b]	

[a]Reference 18.
[b]Reference 32.
[c]Reference 13.
[d]Reference 26.

II. COMPUTATIONAL DETAILS

The structural parameters, formation energy, and elastic properties are calculated by using the WIEN2K package, which is based on the all-electron full potential linearized augmented plane wave (FP-LAPW) method within the framework of density functional theory.[21] The exchange-correlation potentials are treated by both the LDA (Ref. 22) and the Perdew–Burke–Ernzerhof GGA.[23] The lanthanum 6*s*, 5*d*, 5*p*, 5*s*, and 4*f* electrons, the aluminum 3*s* and 3*p* electrons, and the oxygen 2*s* and 2*p* electrons are treated as in the valence states. Relativistic effects are taken into account within the scalar-relativistic approximation in the calculation of the valence states and core levels.[24] The Muffin-tin sphere radii R_{MT} are chosen to be 2.4, 1.6, and 1.6 Bohr for the La, Al, and O atoms, respectively. The numbers of symmetrized k points, used as input for the self-consistent charge density determination, are 65 and 35 k-points in the irreducible symmetry wedge of the Brillouin zone for the rhombohedral and cubic structures, respectively. The maximum l value for the wave function expansion inside the atomic spheres is confined to $l_{max}=10$. A satisfactory convergence is achieved by setting the number of FP-LAPW basis functions to $R_{MT}K_{max}=7$, where K_{max} is the largest reciprocal vector used in the LAPW basis set. The self-consistent calculations are considered to converge when the total energy of the system is stable within 10^{-5} Ry per formula unit.

During the structural geometry optimization, the calculation is based on the experimental study. In doing this we first adopt the experimental data to calculate the a/c ratio and optimize the equilibrium volume, and then we use the theoretical equilibrium volume and optimize the ratio of a/c. After that, the internal atomic configurations are fully relaxed with a constant shape and volume.

III. STRUCTURAL STABILITY AND PHASE TRANSITION

To investigate the stable structure at low temperature, we compare the formation energies of three rhombohedral structures: *R*-3*C* (No. 167), *R*-3*M* (No. 166), and *R*3*C* (No. 161). In the *R*-3*C* structure, the Al atoms are located at −3 sites, La atoms at 32 sites, and O atoms at 2 sites. All the Al atoms are at the center of the AlO_6 octahedra, but the oxygen and La atoms are not longer at the symmetry center due to the oxygen octahedra distortion around the Al atoms. The *R*-3*C* and *R*-3*M* belong to the same crystal class, but the *R*-3*M* would have Al atoms at −3*m* sites, La atoms at 3*m* sites, and O atoms at *m* sites. All the Al atoms in the unit are not equivalent, and the oxygen and La (111) planes are displaced independently along the c axis. If the Al atoms have a small amount of displacement from the center of symmetry during the phase transition, it will shift slightly from the inversion center, and the lack of inversion symmetry will lead to a space group of *R*3*C* instead of *R*-3*C*. The slightly distinguishable site symmetry in the three rhombohedral structures will result in a very different symmetry division of the zone center phonon modes as well as different formation energies.[17] In our calculation, the formation energy is defined as

$$\Delta E = E_{LaAlO_3} - E_{La} - E_{Al} - E_{O}.$$

The formation energies and lattice parameters obtained from the calculations are listed in Table I together with the corresponding experimental results. The lattice parameters are in better agreement with experimental values while using the GGA scheme. As shown in Table I, the *R*-3*C* phase is the most energetically favorable structure because of its relatively lower formation energy compared to the other rhombohedral structures. The formation energy of the *R*-3*M* structure is very close to that of the *PM*-3*M* structure. On the other hand, *R*3*C* is the energy adverse structure due to its relatively high formation energy, Sathe and Dubey[19] observed some weak Raman bands on the left side of the strongest A_1 Raman band in the resonant Raman spectrum at low temperatures. These weak Raman bands are probably originated from the induced vibration of La in the hexagonal (001) plane, which is accompanied with the rotation of the oxygen octahedra, such extra bands are also interpreted as ghost modes in many literatures.[25] The calculated stable structure of *R*-3*C* at low temperature is consistent with the soft mode analysis.[15–17]

It is well known that there is a phase transition from rhombohedral *R*-3*C* to cubic *PM*-3*M* in $LaAlO_3$ when the temperature is above 813 K.[25] Recently, the high pressure investigation showed that $LaAlO_3$ presented structure instabilities and underwent a soft-mode driven rhombohedral to cubic phase transition at high pressure.[26] As shown in Fig. 1, these phase transitions are attributed to the distortion of oxy-

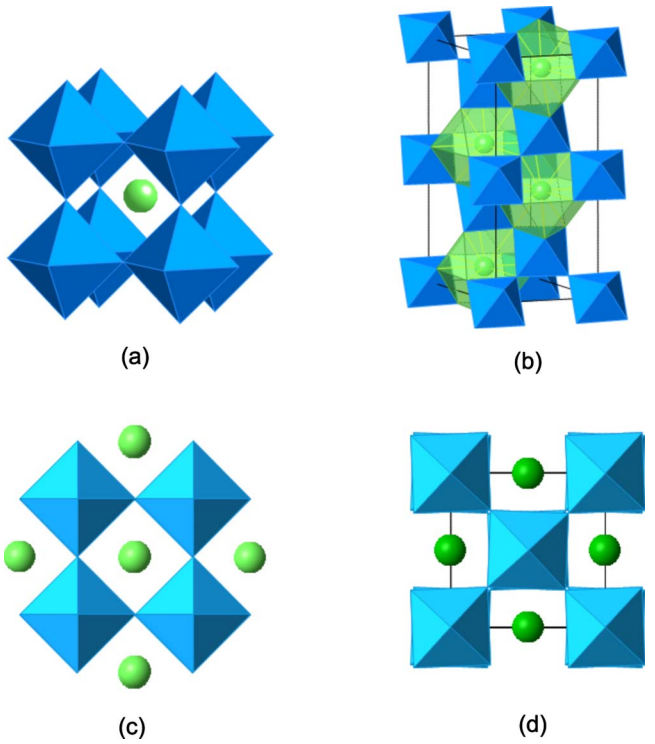

FIG. 1. (Color online) Crystal structure of $LaAlO_3$. The AlO_6 octahedra are shown in dark gray (blue), the LaO_{12} sites are shown in light (green), and the O atoms are in the vertex of polyhedron. (a) $LaAlO_3$ cubic structure (*PM*-3*M*, space group No. 221), (b) $LaAlO_3$ rhombohedral structure (*R*3*C*, space group No. 161), (c) planform of the $LaAlO_3$ cubic structure, and (d) rotation of the AlO_6 octahedra along the [111] direction of rhombohedral $LaAlO_3$.

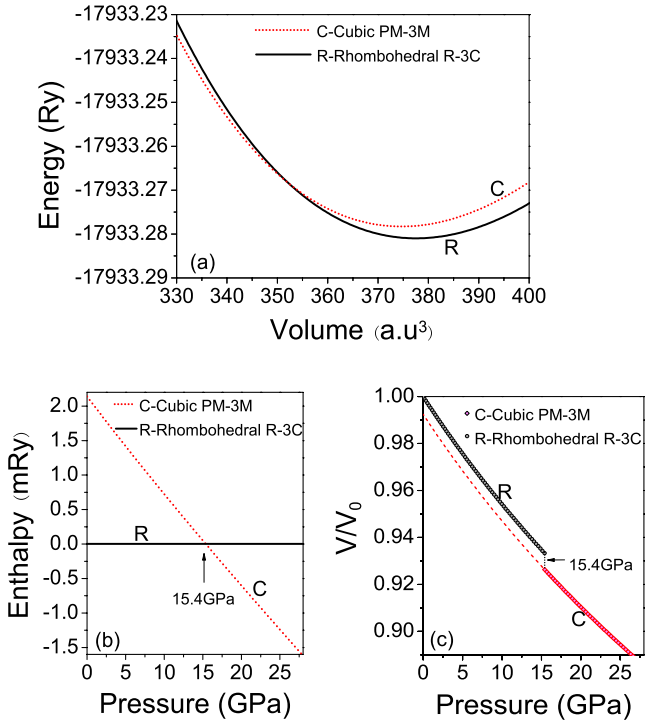

FIG. 2. (Color online) (a) Total energy (E_t) of two structures as a function of cell volume (V). Dotted and solid lines denote the energies for the cubic *PM*-3*M* and rhombohedral *R*-3*C* structures. (b) The stability of *R*-3*C* phase relative to *PM*-3*M* phase as a function of pressure. The transition pressure is marked by arrow at the transition point. (c) Relationship between pressure and volume for the two phases of $LaAlO_3$.

gen octahedral. The corner-linked AlO_6 octahedra form the structural backbone of $LaAlO_3$ perovskite. Below the critical transition point, driven by the rotation of the AlO_6 octahedra along the [111] cubic unit cell direction, the adjacent octahedra rotate in the opposite direction, leading to the structure of rhombohedral *R*-3*C*. In order to get more quantitative analysis of this dynamic phase transition, we use first-principles techniques to analyze the dynamic structural transformation in $LaAlO_3$ under high pressure. Figure 2(a) shows the total energy of the cubic *PM*-3*M* and rhombohedral *R*-3*C* phases as a function of cell volume, where the *R*-3*C* phases are rescaled in the pseudocubic volume. In both phases, the lattice constants and internal positions are relaxed at a set of constant volumes. The calculated relationship between total energy and cell volume is fitted by the Birch–Murnaghan equation:[27]

$$E = E_0 + \frac{9}{16}\left(\frac{B}{14\,703.6}\right)V_0[(\eta^2-1)^3B' + (\eta^2-1)^2(6-4\eta^2)],$$

where $\eta=(V_0/V)^{1/3}$. The calculated values of the bulk modulus B and its pressure derivative B' for $LaAlO_3$, obtained from the fitting of state equation, yield 192.9364 GPa and 4.1506 for *R*-3*C* phase, and 194.0217 GPa and 4.1209 for *PM*-3*M* phase, respectively. Upon decreasing the volume, the lowest energy state shifts from the rhombohedral phase to the cubic phase, and a phase transition is expected to take place at the intersection area from the principle of minimum energy. To determine the transition pressure at zero temperature, only the enthalpy $G=E+PV$ should be considered. For a given pressure, a stable structure is the one for which Gibbs free energy has the lowest value. Hence, the common tangent of the intersection in energy-volume curves indicates the phase transition pressure. The Gibbs free energy difference with respect to the rhombohedral *R*-3*C* phase was shown as a function of pressure in Fig. 2(b), and the pressure is calculated by the relative change of the volume and the bulk modulus:

$$P = \frac{3}{2}B(\eta^7-\eta^5)\left[1+\frac{3}{4}(B'-4)(\eta^2-1)\right].$$

In the pressure induced phase transition, our theoretical calculated pressure is 15.4 GPa in agreement with the experiments value, which is in the vicinity of 14 GPa.[26] Besides that, the relationship between pressure and volume for the two phases is also shown in Fig. 2(c). It is clear that during the transition region, there is a volume change of 1%, which is usually accompanied with the structural phase transition. The calculated value of the volume change still needs further experimental identification.

IV. CALCULATION OF ELASTIC CONSTANTS

The computation of the elastic constants is based on the expansion of total energy in power of the external strain tensor ε.[20] When symmetric distortion strains are applied to the equilibrium unit cell, there will be some changes in the

TABLE II. The elastic constants (GPa), bulk and shear moduli, Young modulus, and Poisson's ratio for the *R*-3*C* and *PM*-3*M* phases of $LaAlO_3$.

	R-3*C*			*PM*-3*M*		
	LDA	GGA	Expt.	LDA	GGA	Expt.[b]
c_{11}	390.70	381.56	337[a]	324.47	313.56	308
c_{33}	411.3	411.17	411[a]			
c_{44}	119.84	115.33	121[a]	169.16	175.61	154
c_{66}	122.34	140.63	93[a]			
c_{12}	146.03	100.30	151[a]	120.65	134.62	129
c_{13}	69.79	72.54	93[a]			
c_{14}	34.56	29.66	46[a]			
B	196.03	185.63	195.76[a] 190[b]	187.94	199.45	192.37
G	133.10	134.92	114.49[a]	137.37	133.67	123.77
E	325.62	325.82	287.43[a]	331.37	327.78	305.73
υ	0.22	0.21	0.26[a]	0.21	0.23	0.24

[a]Reference 30.
[b]Reference 26. The single crystal elastic constants c_{ij} are from the measurement. The bulk modulus *B*, shear modulus *G*, Young modulus *E*, and Poisson's ratio υ are calculated from the experimental elastic constants.

total energy *E*, and the elastic constants can be obtained by fitting a polynomial to the total energy as a function of distortion and then taking the second derivatives $\partial^2 E/\partial\varepsilon^2$.[28] In order to avoid the plastic deformation, the applied perturbed strain must be small. A necessary condition for a crystal to be mechanically stable is that the elastic energy must be positive, or alternatively, its elastic stiffness matrix should satisfy the well-known Born stability criteria.[29] For a trigonal structure, the criteria result in the following conditions:

$$c_{11} - |c_{12}| > 0, \quad (c_{11} + c_{12})c_{33} - 2c_{13}^2 > 0,$$

$$(c_{11} - c_{12})c_{44} - 2c_{14}^2 > 0.$$

And the corresponding mechanical stability conditions for the cubic structure are

$$c_{11} > 0, \quad c_{44} > 0, \quad c_{11} - |c_{12}| > 0, \quad c_{11} + 2c_{12} > 0.$$

The calculated elastic constants tabulated in Table II show that both phases of $LaAlO_3$ are mechanically stable in their respective crystal systems. Our calculated elastic constants can be compared to the experimental data measured by Brillouin spectroscopy and resonant ultrasound spectroscopy.[30] The elastic constants obtained from our LDA calculations are found to compare favorably with the experimental data compared to the GGA calculated values. The deviation of the calculated elastic constants and the experimental values are partially due to the influence of temperature and the factors such as the defect or impurity of the samples. Besides that, since the values of c_{12}, c_{13}, and c_{14} cannot be extracted by the corresponding polynomial fit directly, uncertain errors induced by the associated method may also attribute to the larger deviation in c_{12}, c_{13}, and c_{14}. The elastic constants of c_{11} and c_{33} in *R*-3*C* phase are significantly larger than the other elastic constants, resulting in a pronounced elastic anisotropy that will be discussed later in more detail. The *PM*-3*M* phase of $LaAlO_3$ has higher symmetry compared to *R*-3*C* phase, and except for the elastic constants along the axis, most of the elastic constants in *PM*-3*M* phase are larger than that in *R*-3*C* phase. It is interesting to try to understand the microscopic origin of these phenomena. As demonstrated by Angel *et al.*,[31,32] in ABO_3 perovskites when the *A* and *B* cations have the same charge, the BX_6 octahedra are more compressible than the AX_{12} sites. Both the La and Al cations have the same +3 charge in the $LaAlO_3$, therefore the AlO_6 octahedra are more compressible than the LaO_{12} sites. This can also be inferred from the relative length changes in the calculated La–O and Al–O bonding as listed in Table I. The ratio of the La–O bonding reduction to that of Al–O bonding between the two different phases is 0.8. In the *PM*-3*M* structure, where the La occupies the center of the 12-fold oxygen coordination, there is an array of regular AlO_6 octahedra sharing corners and forms a rigid framework [Fig. 1(a)]. While in the *R*-3*C* structure, the tilting of the AlO_6 will cause an excursion of LaO_{12} and makes the structure softer along most directions, but in certain directions, such as in the crystallographic axis, the AlO_6 is slightly rotating toward the interstice while the LaO_{12} sites are straightened up along the axis [Fig. 1(b)]. As a result of that, the elastic constants of $c_{11}(c_{22})$ and c_{33} increase a lot in *R*-3*C* structure with respect to that in *PM*-3*M* structure.

Most of the time, it is impossible to measure the individual elastic constants when single crystals are not available, however, the bulk modulus *B* and shear modulus *G* can be measured to determine its elastic properties. On the scheme of Voigt[33] and Reuss[34] and with the approximation of Hill's[35] arithmetic average, we calculated the bulk modulus *B* and shear modulus *G* listed in Table II. Furthermore, the Young modulus *E* and Poisson's ratio υ have been calculated with the following equations for the isotropic material:

$$E = 9BG/(3B + G), \quad \upsilon = (3B - 2G)/2(3B + G).$$

As a result, the calculated bulk modulus from the average of LDA and GGA value is 193.70 GPa for the *PM*-3*M* phase, slightly larger than the value 190.83 GPa for the *R*-3*C* phase. These bulk modulus values are found to be consistent with the one obtained from previous equation of state studies as well as the high-pressured measurements.[26] The Poisson ratio υ, which is associated with the transverse strain under

TABLE III. Debye temperature, anisotropic factor, and directional bulk moduli of $LaAlO_3$ and SiO_2.

	R-3*C*			*PM*-3*M*			$SiO_2(\alpha)$
	LDA	GGA	Expt.	LDA	GGA	Expt.[a]	GGA
$\rho(g/cm^3)$	6.53	6.50	6.52[a] 6.70[b]	6.54	6.73	6.58	2.65
$v_m(m/s)$	4997.72	5033.31	4654.09[a]	5062.88	4933.19	4805.51	4710.39
$\Theta_D(K)$	671.97	675.83	625.60[a] 748[b]	681.16	670.16	647.94	469.02
A_1	0.72	0.71	0.86[a]	1.66	1.96	1.72	1.46
A_2	1	1	1[a]				1
A_{B_a}	1	1	1[a]				1
A_{B_c}	0.86	1.01	1.05[a]				0.89
$A_B(\%)$	−0.02	−0.34	−2.60 [a]	0.35	−2.60	−1.92	0.95
$A_G(\%)$	−0.17	0.94	5.60[a]	3.56	5.60	3.58	1.83

[a]Reference 31. Calculated from the experimental single crystal elastic constants of M.A. Carpenter.
[b]Reference 39.

uniaxial press, was obtained as 0.22. The quotient of bulk to shear modulus (B/G) is roughly considered as a criteria to judge the brittle properties,[36] the critical value is 1.75, above that the material is regarded as ductile. The calculated B/G value for $LaAlO_3$ is 1.46, suggesting that $LaAlO_3$ is brittle.

V. DEBYE TEMPERATURE AND ELASTIC ANISOTROPY

As mentioned before, the $LaAlO_3$ is considered as a promising candidate of the high k gate oxide to replace the SiO_2. It is required to be thermostable and durable to resist the dielectric breakdown. In order to get more insight, the Debye temperature and elastic anisotropy are both examined and listed in Table III.

Debye temperature Θ_D is the temperature of a crystal's highest normal mode of vibration, and it correlates the elastic properties with the thermodynamic properties such as phonons, specific heat, thermal expansion, thermal conductivity, and lattice vibration enthalpy. At low temperature, the contributions to specific heat mainly come from the vibration of lowest temperature acoustic mode. The estimated Debye temperature Θ_D from the elastic constants is valid as compared to those values determined by the heat capacity measurements.[37] The Debye temperature can be calculated from the averaged elastic-wave velocity in the following equation:[38]

$$\Theta_D = \frac{h v_m}{k}\left[\frac{3n}{4\pi}\left(\frac{N_A \rho}{M}\right)\right]^{1/3},$$

where h is Planck's constant, k is Boltzmann's constant, N_A is Avogadro's number, n is the number of atoms in unit cell, ρ is the density, M is the weight of unit cell, and v_m is the averaged wave velocity integrated over several crystal directions

$$v_m = \left[\frac{1}{3}\left(\frac{2}{v_t^3} + \frac{1}{v_l^3}\right)\right]^{-1/3},$$

where v_t and v_l are the transverse and longitudinal elastic waves of the $LaAlO_3$. They are obtained by

$$v_l = \left(\frac{B + 4G/3}{\rho}\right)^{1/2}, \quad v_t = (G/\rho)^{1/2}.$$

The Debye temperatures for most crystals are around 200–400 K. The computed values of Debye temperatures Θ_D are 675 and 670 K for the *R*-3*C* and *PM*-3*M* phases of $LaAlO_3$, respectively, indicating that $LaAlO_3$ is hard with a large wave velocity. From Table III, it is interesting to note that the Debye temperatures calculated from acoustic phonons are a little bit smaller than the value 748 K estimated from the low temperature specific heat measurement.[39] One of the possible reasons for such a discrepancy between the experimental and calculated data is the presence of excess specific heat, which is from the contribution of low-frequency optical phonons and Einstein harmonic oscillator. Insulators transfer heat by lattice vibrations in terms of phonon, and the density and velocity of these phonon gases depend on the Debye temperature. Therefore, the thermal conductivity of the $LaAlO_3$ in both phases is expected to be high compared to normal dielectrics, and the thin $LaAlO_3$ gate oxide film is predicted to be more heat resistant.

The dielectric breakdown in the electronic device is not only related to the thermal burnout, but also to the micro crack and dislocations induced by the anisotropy of thermal expansion and elastic deformation.[40] The calculation of the elastic anisotropy is well established in the crystal physics. The elastic anisotropy arises from both shear anisotropy and the anisotropy of linear bulk modulus. For trigonal materials, the shear anisotropic factors for {100} shear plane in ⟨010⟩ and ⟨011⟩ directions are[20]

$$A_1 = 4c_{44}/(c_{11} + c_{33} - 2c_{13})$$

and for {001} shear plane in ⟨010⟩ and ⟨110⟩ direction are

$$A_2 = 2c_{66}/(c_{11} - c_{12}).$$

The shear anisotropic factor of {010} plane is the same as that of {100} shear plane due to the symmetry imposed by its crystal group. In the cubic crystals, the shear anisotropic factors have the same value in its three shear plane. For isotropic crystal the value of A_1 and A_2 should be one, and any

deviation of unity is a measure of its elastic anisotropy. From our calculation shown in Table III, the factor A_1 is smaller than unity in the R-3C phase, reflecting the more pronounced directional bonding charge density between atoms in {100} planes. This is because the AlO_6 octahedral tilting has significant influence in the bonding in those planes. In addition, the PM-3M phase of the $LaAlO_3$ has pronounced anisotropic properties compared to R-3C phase.

In order to investigate the contribution of the linear bulk modulus to the elastic anisotropy of $LaAlO_3$, we calculated the bulk modulus along the crystal axes,[20] defined as $B_i = idP/di$, $(i=a,b,c)$. The compressibility anisotropy of bulk modulus along a and c axes with respect to b axis can then be written as $A_{B_a}=B_a/B_b$ and $A_{B_c}=B_c/B_b$. For these two parameters, a value of unity represents elastic isotropy and any deviation from one indicates the degree of the elastic anisotropy. However, in the cubic crystals, the linear bulk modulus is the same for all directions, and the compressibility anisotropy is not applied. To overcome this limitation, Chung and Buessem[41] introduced a more practical measure of elastic anisotropy called percentage elastic anisotropy. The percentage anisotropy in compressibility and shear are defined as $A_B=(B_V-B_R)/(B_V+B_R)$ and $A_G=(G_V-G_R)/(G_V+G_R)$, respectively, where B and G are bulk and shear modulus, and the subscripts V and R represent the Voigt[33] and Reuss[34] schemes. For the percentage anisotropy, a value of zero indicates the elastic isotropy and a value of 100% identifies the largest possible anisotropy.

The calculated values of the anisotropy percentage are also given in Table III. It is seen that the R-3C phase of the $LaAlO_3$ is slightly isotropic in nature, and the experimental percentage anisotropy shows a higher degree of anisotropy than the values obtained from theoretical calculations. Moreover, it is interesting to note that the PM-3M phase of the $LaAlO_3$ has higher anisotropy in the criteria of percentage anisotropy.

We compared the Debye temperature and elastic anisotropy with the traditional gate oxides SiO_2. The Debye temperature of SiO_2 is 469 K and its anisotropy factors are larger than those of the $LaAlO_3$. These results show that the $LaAlO_3$ is superior to the SiO_2 in the aspect of resisting dielectric breakdown.

VI. CONCLUSIONS

In summary, we have used the FP-LAPW method to study the disputed low temperature structure of the $LaAlO_3$, and found that the R-3C is the most energetically stable structure among the structures: R-3M, R-3C, and $R3C$. A pressure induced phase transition in $LaAlO_3$ is investigated, and the calculated phase transition pressure from rhombohedral R-3C phase to cubic PM-3M phase is at 15.4 GPa, which is in agreement with the high-pressure experimental value. We also calculated the elastic constants by using the strain perturbation method and found that the constants calculated with LDA scheme are in better agreement with the experimental data. It is shown that the rotation of the AlO_6 octahedra in R-3C phase has significant influence on the directional elastic constants, and it can be used to explain the different characters in elastic constants for the two phases of $LaAlO_3$. The calculated Debye temperature and elastic anisotropic factors indicated that the R-3C phase of $LaAlO_3$ is more thermostable and has higher fracture toughness.

ACKNOWLEDGMENTS

The authors thank Michael Carpenter for providing the experimental data of elastic constants and stimulating discussions. This work was supported by the National Natural Science Foundation of China (Grant Nos. 10732100 and 10572155) and the Guangdong Science and Technology Bureau (Grant No. 2006A11001002).

[1] N. Reyren, S. Thiel, A. D. Caviglia, L. F. Kourkoutis, G. Hammerl, C. Richter, C. W. Schneider, T. Kopp, A. S. Ruetschi, D. Jaccard, M. Gabay, D. A. Muller, J. M. Triscone, and J. Mannhart, Science **317**, 1196 (2007).
[2] Y. K. Yoo, F. Duewer, H. T. Yang, D. Yi, J. W. Li, and X. D. Xiang, Nature (London) **406**, 704 (2000).
[3] M. S. Dilorio, S. Yoshizumi, M. Maung, K. Y. Yang, J. Zhang, and N. Q. Fan, Nature (London) **354**, 513 (1991).
[4] A. E. Lee, C. E. Platt, J. F. Burch, R. W. Simon, J. P. Goral, and M. M. Al-Jassim, Appl. Phys. Lett. **57**, 2019 (1990).
[5] The International Technology Roadmap for Semiconductor, 2007, http://public.itrs.net
[6] J. Robertson, Rep. Prog. Phys. **69**, 327 (2006).
[7] B. E. Park and H. Ishiwara, Appl. Phys. Lett. **82**, 1197 (2003).
[8] S. G. Lim, S. Kriventsov, T. N. Jackson, J. H. Haeni, D. G. Schlom, A. M. Balbashov, R. Uecker, P. Reiche, J. L. Freeouf, and G. Lucovsky, J. Appl. Phys. **91**, 4500 (2002).
[9] W. Xiang, H. Lü, L. Yan, H. Guo, L. Liu, Y. Zhou, G. Yang, J. Jiang, H. Cheng, and Z. Chen, J. Appl. Phys. **93**, 533 (2003).
[10] Y. Y. Mi, Z. Yu, S. J. Wang, P. C. Lim, Y. L. Foo, A. C. H. Huan, and C. K. Ong, Appl. Phys. Lett. **90**, 181925 (2007).
[11] D. O. Klenov, D. G. Schlom, H. Li, and S. Stemmer, Jpn. J. Appl. Phys., Part 2 **44**, L617 (2005).
[12] E. A. Wood, Am. Mineral. **36**, 768 (1951).
[13] S. Geller and V. B. Bala, Acta Crystallogr. **9**, 1019 (1956).
[14] G. W. Berkstresser, A. J. Valentino, and C. D. Brandle, J. Cryst. Growth **109**, 457 (1991).
[15] W. Cochran, Phys. Status Solidi **25**, 273 (1968).
[16] K. A. Müller, W. Berlinger, and F. Waldner, Phys. Rev. Lett. **21**, 814 (1968).
[17] J. F. Scott, Phys. Rev. **183**, 823 (1969).
[18] C. J. Howard, B. J. Kennedy, and B. C. Chakoumakos, J. Phys.: Condens. Matter **12**, 349 (2000).
[19] V. G. Sathe and A. Dubey, J. Phys.: Condens. Matter **19**, 382201 (2007).
[20] P. Ravindran, L. Fast, P. A. Korzhavyi, B. Johansson, J. Wills, and O. Eriksson, J. Appl. Phys. **84**, 4891 (1998).
[21] P. Blaha, K. Schwarz, G. Madsen, D. Kvasnicka, and J. Luitz, *WIEN2k, An Augmented Plane Wave Plus Local Orbitals Program for Calculating Crystal Properties* (Vienna University of Technology, Vienna, 2001).
[22] J. P. Perdew and Y. Wang, Phys. Rev. B **46**, 12947 (1992).
[23] J. P. Perdew, K. Burke, and M. Ernzerhof, Phys. Rev. Lett. **77**, 3865 (1996).
[24] D. D. Koelling and B. N. Harmon, J. Phys. C **10**, 3107 (1977).
[25] S. A. Hayward, F. D. Morrison, S. A. T. Redfern, E. K. H. Salje, J. F. Scott, K. S. Knight, S. Tarantino, A. M. Glazer, V. Shuvaeva, P. Daniel, M. Zhang, and M. A. Carpenter, Phys. Rev. B **72**, 054110 (2005).
[26] P. Bouvier and J. Kreisel, J. Phys.: Condens. Matter **14**, 3981 (2002).
[27] F. D. Murnaghan and A. J. Math, Proc. Natl. Acad. Sci. U.S.A. **30**, 244 (1944).
[28] D. C. Wallace, *Thermodynamics of Crystals* (Dover, New York, 1998).
[29] F. I. Fedorov, *Theory of Elastic Waves in Crystals* (Plenum, New York, 1968).
[30] M. A. Carpenter, T. W. Darling, J. D. Bass, D. L. Lakshtanov, S. V.

Sinogeikin, and S. D. Jacobsen, American Geophysical Union Fall Meeting, 2006 (unpublished).
[31]R. J. Angel, J. Zhao, and N. L. Ross, Phys. Rev. Lett. **95**, 025503 (2005).
[32]J. Zhao, N. L. Ross, and R. J. Angel, J. Phys.: Condens. Matter **16**, 8763 (2004).
[33]W. Voigt, *Lehrbuch der Krystallphysik* (Verlag und Druck BG Teubner, Leipzig, 1928).
[34]A. Reuss, Z. Angew. Math. Mech. **9**, 49 (1929).
[35]R. Hill, Proc. Phys. Soc. London **65**, 349 (1952).
[36]S. F. Pugh, Philos. Mag. **45**, 823 (1954).
[37]M. Born and K. Huang, *Dynamical Theory of Crystal Lattices* (Oxford University Press, New York, 1998).
[38]O. L. Anderson, J. Phys. Chem. Solids **24**, 909 (1963).
[39]W. Schnelle, R. Fischer, and E. Gmelin, J. Phys. D **34**, 846 (2001).
[40]V. Tvergaard and J. W. Hutchinson, J. Am. Ceram. Soc. **71**, 157 (1988).
[41]D. H. Chung and W. R. Buessem, in *Anisotropy in Single Crystal Refractory Compounds*, edited by F. W. Vahldiek and S. A. Mersol (Plenum, New York, 1968).